



HAL
open science

Dual Photoredox Ni/Benzophenone Catalysis: A Study of the Ni II Precatalyst Photoreduction Step

Axel Almansa, Damien Jardel, Stéphane Massip, Thierry Tassaing, Christophe Schatz, Jérémy Domergue, Florian Molton, Carole Duboc, Jean-Marc Vincent

► **To cite this version:**

Axel Almansa, Damien Jardel, Stéphane Massip, Thierry Tassaing, Christophe Schatz, et al.. Dual Photoredox Ni/Benzophenone Catalysis: A Study of the Ni II Precatalyst Photoreduction Step. *Journal of Organic Chemistry*, 2022, 87 (16), pp.11172-11184. 10.1021/acs.joc.2c01467 . hal-03842489

HAL Id: hal-03842489

<https://hal.science/hal-03842489v1>

Submitted on 7 Nov 2022

HAL is a multi-disciplinary open access archive for the deposit and dissemination of scientific research documents, whether they are published or not. The documents may come from teaching and research institutions in France or abroad, or from public or private research centers.

L'archive ouverte pluridisciplinaire **HAL**, est destinée au dépôt et à la diffusion de documents scientifiques de niveau recherche, publiés ou non, émanant des établissements d'enseignement et de recherche français ou étrangers, des laboratoires publics ou privés.

Dual Photoredox Ni/Benzophenone Catalysis: A Study of the Ni^{II} Precatalyst Photoreduction Step

*Axel Almansa, Damien Jardel, Stéphane Massip, Thierry Tassaing, Christophe Schatz, Jérémy Domergue, Florian Molton, Carole Duboc and Jean-Marc Vincent**

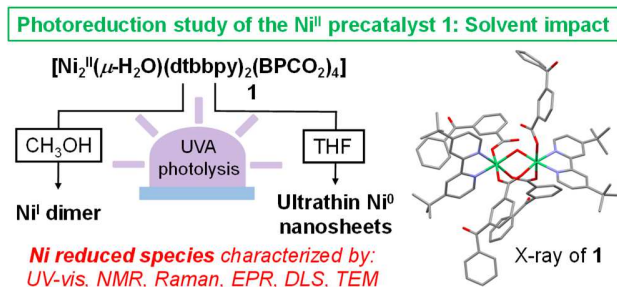
Axel Almansa, Damien Jardel, Thierry Tassaing, Jean-Marc Vincent - Institut des Sciences Moléculaires (ISM), CNRS UMR 5255, Univ. Bordeaux, 33405 Talence, France

Stéphane Massip - European Institute of Chemistry and Biology (IECB), Univ. Bordeaux, 33600 Pessac, France

Christophe Schatz - Laboratoire de Chimie des Polymères Organiques (LCPO), CNRS UMR 5629, Univ. Bordeaux, 33607 Pessac Cedex, France

Florian Molton, Jérémy Domergue, Carole Duboc - Département de Chimie Moléculaire (DCM) CNRS UMR 5250, Univ. Grenoble Alpes, F-38000 Grenoble, France

KEYWORDS: nickel, benzophenone, photoredox catalysis, cross-coupling, ultrathin metallic nanosheet



ABSTRACT: The combination of Ni^{II}X₂ salts with a bipyridine-type ligand and aromatic-carbonyl-based chromophores has emerged as a benchmark precatalytic system to efficiently conduct cross-couplings mediated by light. Mechanistic studies have led to two scenarios in which Ni⁰ is proposed as the catalytic species. Nonetheless, in none of these studies a Ni^{II} to Ni⁰ photoreduction has been evidenced. By exploiting UV-visible, nuclear magnetic resonance (NMR), resonance Raman, electron paramagnetic resonance (EPR) and dynamic light scattering (DLS) spectroscopies, and also transmission electron microscopy (TEM), we report that when photolyzed by UVA in alcohols, the structurally-defined [Ni^{II}₂(μ-OH₂)(dtbbpy)₂(BPCO₂)₄] complex **1** integrating a benzophenone chromophore is reduced into a diamagnetic Ni^I dimer of general formula [Ni^I₂(dtbbpy)₂(BPCO₂)₂]. In marked contrast, in THF, photolysis led to the fast formation of Ni⁰, which accumulates in the form of metallic ultrathin Ni nanosheets characterized by a mean size of ~ 100 nm and a surface plasmon resonance at 505 nm. Finally, it is shown that **1** combined with UVA irradiation catalyzes cross-couplings, i.e. a C(sp³)-H arylation of THF and a O-arylation of methanol. These results are discussed in light of the mechanisms proposed for these cross-couplings, with a focus on the oxidation state of the catalytic species.

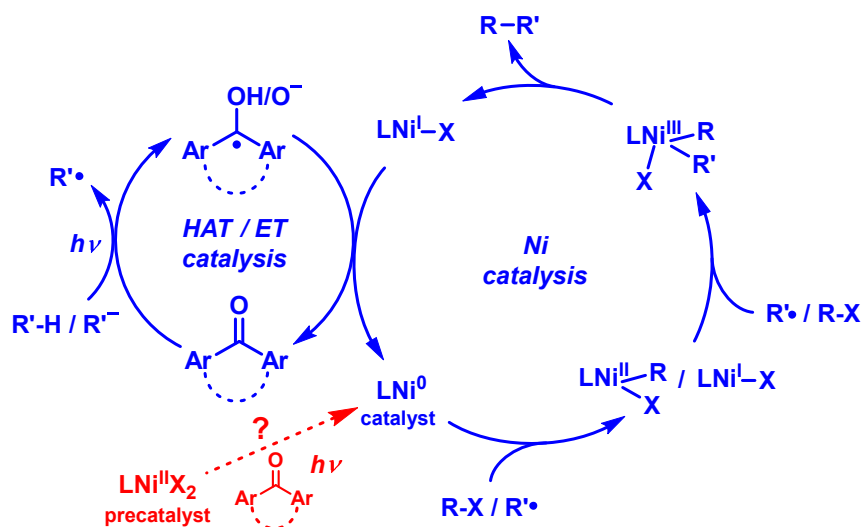
INTRODUCTION

Dual photoredox/Ni catalysis is the subject of intense researches that have led to the discovery of highly effective carbon-carbon and carbon-heteroatom cross-coupling reactions.^{1,2} While Ir complexes have been the most widely employed photoredox catalysts in these processes,^{3,4} the use of organic photoredox catalysts,⁵⁻⁷ in particular aromatic carbonyl derivatives,^{5,6c-f} is receiving increasing interest as promising alternatives to noble and rare metal-based complexes.

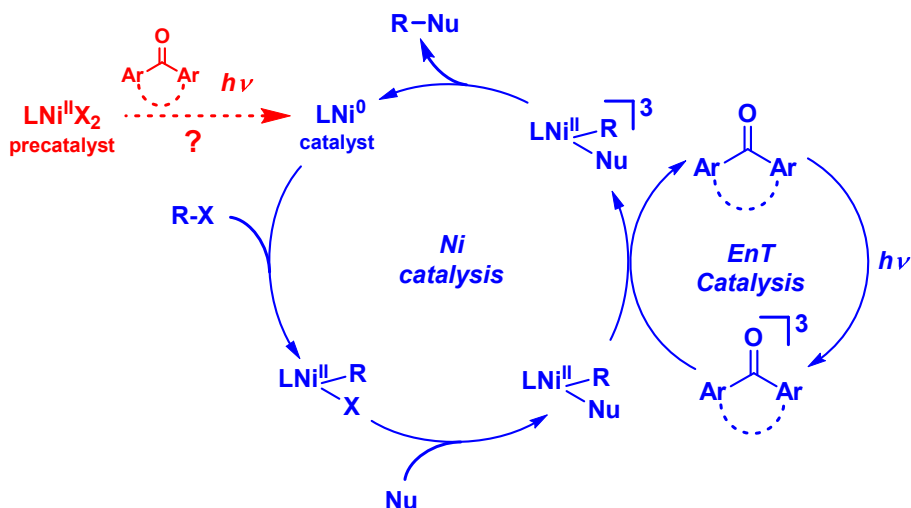
Over the last five years, great efforts have been devoted to the elucidation of the reaction mechanisms involved in these dual photoredox/Ni catalyzed processes, particularly in the Ir/Ni ones.^{1c,1d,8-10} These studies highlighted that deciphering the chemical nature of the reactive species implied in dual photoredox/Ni catalyzed processes is a challenging issue. This is particularly true when structurally ill-defined precatalysts, typically generated *in situ* from NiX₂ (X = Cl, Br) and one or two equivalents of a 2,2'-bipyridine (bpy) ligand, most often the 4,4'-Di-*tert*-butyl-2,2'-dipyridyl (dtbbpy), are irradiated in the presence of photoredox catalysts in rather complex reaction mixtures. Under such conditions, many competing processes may occur, including single electron transfers from photocatalyst excited states, *in situ* generated ketyl radicals, Niⁿ⁺ comproportionation/disproportionation reactions, photoreductive elimination processes from the Ni-halogen precursors/intermediates, trapping of organic radicals by the low-valent Ni^{0/I} species, or generation of long-lived triplet excited states of L_nNi^{II} through direct light excitation or triplet-triplet energy transfer from photocatalyst excited states. A key finding of these studies is that the bpyNi^IX species can effectively perform the oxidative addition steps, and that the C-heteroatom cross-coupling reactions most likely proceed through a dark, thermally sustained Ni^I/Ni^{III} cycle.⁹

Scheme 1. The current two proposed mechanisms for C-C and C-heteroatom photocatalyzed cross-couplings employing bpy/ $\text{Ni}^{\text{II}}\text{X}_2$ /aromatic ketone precatalytic systems. In blue: where previous mechanistic studies have focused. In red: precatalyst activation step explored in this study.

a) General mechanism proposed by Martin,^{6c} Rueping,^{6d,6i} Molander^{6j} and Li.^{7e,7g}



b) General mechanism proposed by Li.^{6k,7f,7h}



Ni^0 has never been directly evidenced, neither under catalytic conditions, nor under photolysis of the $\text{LNi}^{\text{II}}\text{X}_2$ precatalyst.

As far as cross-couplings involving LNiX_2 /aromatic carbonyl couples are concerned (L = bpy derivative), there are no reports focusing on the initial precatalyst photoreduction (Scheme 1). Indeed, the mechanistic studies focused on the elucidation of the different steps of the catalytic cycles, which led to propose two types of mechanism. One implies the interplay of a photo-HAT/photoredox cycle with a Ni catalytic cycle implying $\text{Ni}^0/\text{Ni}^{\text{II}}/\text{Ni}^{\text{III}}/\text{Ni}^{\text{I}}$ or $\text{Ni}^0/\text{Ni}^{\text{I}}/\text{Ni}^{\text{III}}/\text{Ni}^{\text{I}}$ intermediates depending whether the photogenerated radical is reacting with Ni(0) before or after the oxidative addition step. In the other, the triplet sensitization of the $\text{LNi}^{\text{II}}(\text{R})(\text{Nu})$ intermediate allows the reductive elimination step. Rather surprisingly, although in all the proposed reaction mechanisms LNi^0 is the catalytic species, no direct experimental evidence is available regarding its generation, neither under the catalytic conditions, nor during the photolysis of the LNiX_2 /aromatic ketone precatalytic system. What is the oxidation state and the structure of the main reduced species that are generated upon photolysis of the bpyNiX_2 precatalyst in the presence of an aromatic ketone and a reducing agent? What is the efficiency of the reduction process? These are the fundamental questions we address in this study.

Herein, we report the synthesis and characterization of a well-defined precatalyst model, the $[\text{Ni}^{\text{II}}_2(\mu\text{-OH}_2)(\text{dtbbpy})_2(\text{BPCO}_2)_4]$ complex **1** ($\text{BPCO}_2 = 3\text{-benzoylbenzoate}$), and a thorough study of its reduction when photolyzed by UVAs in MeOH, *i*-PrOH or THF. UV-visible, nuclear magnetic resonance (NMR), resonance Raman, electron paramagnetic resonance (EPR) and dynamic light scattering (DLS) spectroscopies, and also transmission electron microscopy (TEM), have been employed to characterize the reduced species. We show that photolysis of **1** in H-atom donating alcohols mainly leads to the diamagnetic $[\text{Ni}^{\text{I}}(\text{dtbbpy})(\text{BPCO}_2)]_2$ dimer, while photolysis in THF generates Ni^0 which accumulates in the form of ultrathin metallic Ni nanosheets of an average size of about 100 nm. Finally, catalytic studies demonstrate that **1** combined with UVA

irradiation catalyzes cross-couplings, i.e. a C(sp³)-H arylation of THF and a O-arylation of methanol.

RESULTS AND DISCUSSION

Synthesis, X-ray and electrochemical characterization of complex 1. By exploiting a synthetic strategy that we developed for the development of photolabile Cu^{II} catalysts,¹¹⁻¹³ the complex **1** was prepared in MeOH by reacting NiSO₄·6H₂O with 1 equiv. of dtbbpy and 2 equiv. of the 3-benzoylbenzoate sodium salt. Faint blue crystals (needles) could be grown by slow diffusion of hexane layered on a THF solution of **1**. The X-ray structure (Figure 1, table S1) reveals that **1** has a dimeric structure, in which octahedral Ni^{II} ions ($d_{\text{Ni}\cdots\text{Ni}}$ 3.52 Å) are bridged by a water molecule and two BPCO₂ in a *syn-syn* configuration, while one dtbbpy and one monodentate BPCO₂ complete the coordination sphere of each Ni^{II} ion. The dimeric structure is further stabilized by intramolecular hydrogen bonds between the carbonyles of the monodentate carboxylates and the bridging water molecule ($d_{\text{O}\cdots\text{O}}$ = 2.54 Å). Comparison of the cyclic voltammogram (CV) of **1** recorded in CH₃CN to those of the dtbbpy ligand and benzophenone shows that a two-electron Ni^{II}/Ni⁰ reduction process occurs at ~ -1.7 V vs Fc/Fc⁺ (Figure S2), in good agreement with previous values reported for [dtbbpyNi^{II}Cl₂].^{4d} The reduction of the benzophenone and dtbbpy in **1** were found at ~ -2.3 V and -2.8 V vs Fc/Fc⁺, respectively.

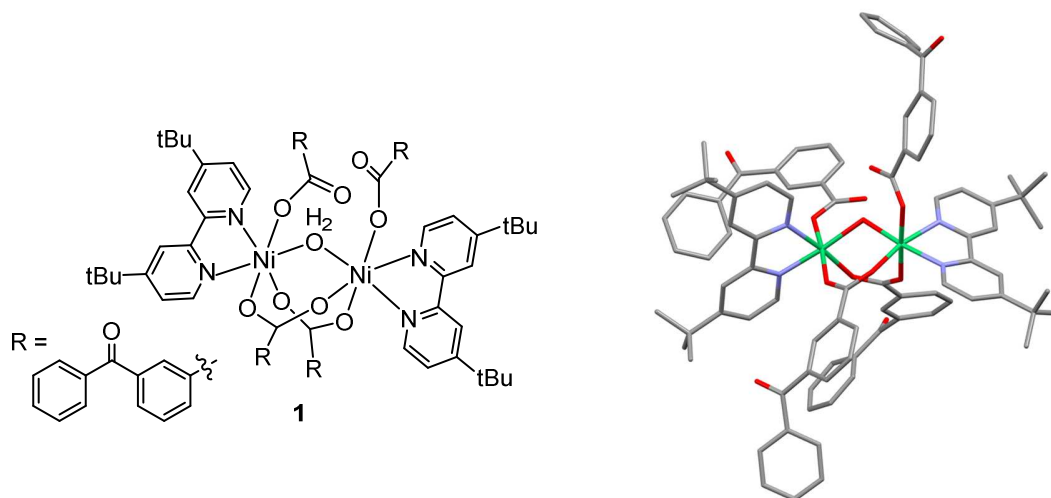


Figure 1. Schematic representation and crystal structure of **1**. Hydrogen atoms and disorder were omitted for clarity.

Photoreduction studies. In the present work, we mostly focus on photoreductions conducted in MeOH, i-PrOH or THF because they are good terminal electron sources in photoredox reducing processes implying hydrogen atom abstraction (HAA), but also because C-O cross-couplings of alcohols^{4a,4h,8a} and C-C cross-couplings of ethers^{6c,6e,6k} are important applications of photoredox (bpy)Ni-catalyzed reactions.

Photolysis in MeOH. Irradiating a strictly deoxygenated MeOH solution of **1** with a low pressure Hg lamp type TLC (TLC = Thin Layer Chromatography, see figure S3) leads to a rapid color change from colorless to dark purple. The UV-Vis follow-up shows that after ~ 30 min of irradiation a new species displaying strong bands at 550 nm and 350 nm is formed (Figure 2). These broad and intense electronic transitions are characteristic of metal to ligand charge transfer (MLCT) bands observed in $[\text{Ni}^{\text{I}}(\text{dtbbpy})]^+$ complexes.^{9b,9c} The accumulating species proved to be extremely reactive towards O_2 , instantaneous discoloration occurring under oxygenation of the solution. When kept under inert atmosphere at room temperature, this species is moderately stable,

with a 45 % linear decrease of the absorbance at 550 nm observed in 14 h (Figure S4). Overall, these observations bode well for the formation of low valent Ni^I or Ni⁰ species. Noticeably, a similar behavior is observed when conducting the photoreduction in *i*-PrOH, i.e. the accumulation of a colorful species exhibiting a similar UV-Vis spectrum, albeit the two main transitions are red-shifted to 360 nm and 595 nm (i.e. by about 10 and 45 nm, respectively, Figure S5). The observed bathochromic shifts with polarity decrease of the solvent agree with the charge-transfer character for these transitions.

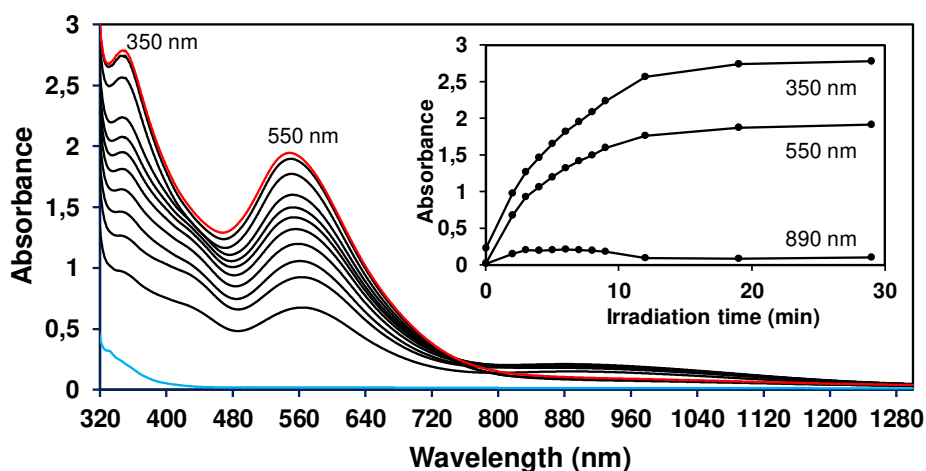


Figure 2. UV-Vis spectra of a MeOH solution (quartz cuvette, path length 1 cm, solution degassed by freeze-pump thaw cycles followed by blowtorch sealing) of **1** (0.25 mM, blue spectrum) after 2, 3, 4, 5, 6, 7, 8, 9, 12, 19 and 29 min of irradiation (TLC lamp placed at 1 cm of the cuvette); Insert: Evolution of the three main bands maxima with time.

A closer look to the spectra in figure 2 reveals that a transient species is observed. This species, characterized by a very broad absorption centered at ~ 890 nm, reaches a maximum concentration from ~ 3 to 10 min of irradiation and then disappears, while the main absorbing species accumulates. Such a broad band at low energy is characteristic of an intervalence transition found

in mixed-valence binuclear complexes. Krüger and Holm have reported on the mixed-valent $\text{Ni}^{\text{I}}\text{Ni}^{\text{II}}$ $[\text{Ni}(\text{pdmt})]_2^-$ species (pdmt = pyridine-2,6-dimethanethiol) that exhibits a broad electronic absorption band centered at 910 nm, and an EPR signal at $\sim g = 2$ ($S = 1/2$) arising from an antiferromagnetic coupling between the two Ni ions.¹⁴ The observation of a transient $S = 1/2$ EPR spectrum associated to a Ni^{I} -based species observed under irradiation of complex **1** in MeOH (See figure 5a and associated discussion) supports the assignment of this transient species to a $\text{Ni}^{\text{I}}\text{Ni}^{\text{II}}$ dimeric complex.

In order to assess whether the intense bands are due to MLCT, but also to determine the Ni oxidation state of the main absorbing species, resonance Raman spectroscopy has been used. Indeed, from the UV-Vis data, one cannot completely rule out that these bands could be the signature of BP or dtbbpy radical anions, which could be formed by single electron transfer (SET) from highly reducing species, in particular Ni^0 . As expected, the complex **1** is Raman silent at a concentration of 2 mM in MeOH and $\lambda_{\text{exc}} 532$ nm (Figure 3a), the only bands observed being those of MeOH. In marked contrast, the spectrum of the colorful dark blue solution recorded after 50 min irradiation exhibits three intense bands at 1613 cm^{-1} , 1538 cm^{-1} and 1476 cm^{-1} , and two less intense at 1313 cm^{-1} and 1285 cm^{-1} . A similar spectrum, albeit less intense, was recorded upon excitation at 633 nm (Figure S6), i.e. under pre-resonant conditions if one considers the electronic absorption band centered at 550 nm. The Raman spectrum is characteristic of those of 2,2'-bipyridine and derivatives. For instance, the Raman spectrum of $[\text{Ru}(\text{bpy})_3]^{2+}$,¹⁵ recorded under resonant conditions with the Ru^{II} to bpy charge-transfer, is characterized by intense bands at 1607 cm^{-1} , 1563 cm^{-1} , 1490 cm^{-1} , 1321 cm^{-1} and 1277 cm^{-1} while the spectrum of the dtbbpy ligand that we recorded at high concentration in THF (0.5 M) exhibits main bands at 1609 cm^{-1} , 1550 cm^{-1} , 1430 cm^{-1} , 1318 cm^{-1} and 1297 cm^{-1} (Figure S7). Conclusive evidence that the band at 550

nm originates from a low valent Ni species to a dtbbpy ligand charge-transfer was obtained by recording the resonance Raman spectrum of $[\text{Cu}(\text{dtbbpy})_2]\text{PF}_6$, for which a Cu^{I} to dtbbpy charge-transfer band is observed at 440 nm. As shown in the Figure 3a, its Raman spectrum, with bands 1610 cm^{-1} , 1543 cm^{-1} , 1473 cm^{-1} , 1311 cm^{-1} and 1290 cm^{-1} , is almost superimposable to that of the final reduced Ni species.

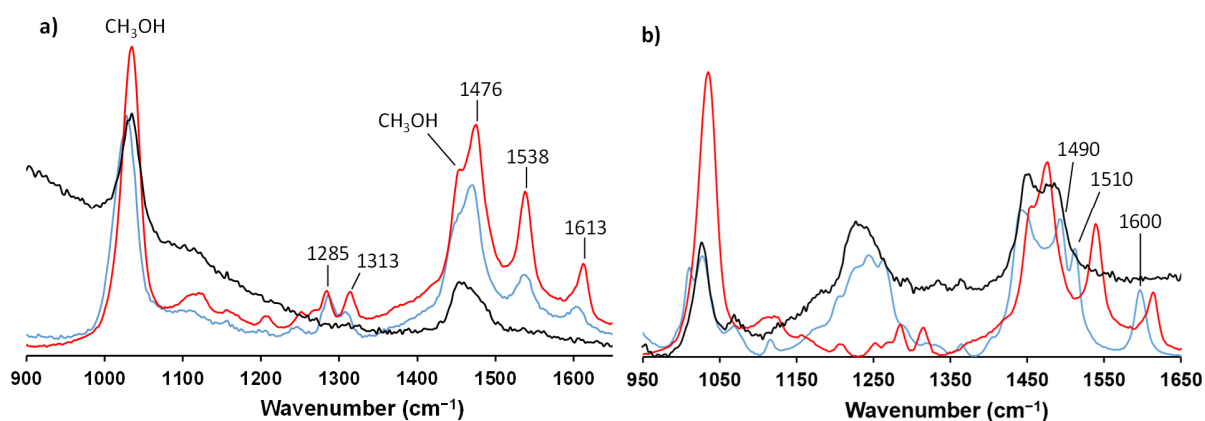


Figure 3. a) Resonance Raman spectra (λ_{exc} 532 nm) of a MeOH solution of **1** (1 mM, 3 mL, UV cuvette, solution degassed by argon bubbling) before (black spectrum) and after (red spectrum) 50 min irradiation at 320-390 nm (TLC lamp set at 365 nm placed at ~ 1 cm of the cuvette); In blue, the resonance Raman spectrum (λ_{exc} 532 nm) of $[\text{Cu}(\text{dtbbpy})_2]\text{PF}_6$ prepared *in situ* by mixing under inert atmosphere $[\text{Cu}(\text{CH}_3\text{CN})_4]\text{PF}_6$ (10 mM) in MeOH with 2 equiv of ligand in MeOH (3 mL degassed by argon bubbling). b) Resonance Raman spectra (λ_{exc} 532 nm) of THF (black spectrum) and a THF-d8 solution of $[\text{Ni}(\text{dtbbpy})\text{COD}]$ in a NMR tube (blue spectrum) prepared following the procedure of ref 3c, compared to the spectrum of the MeOH solution of **1** recorded after 50 min irradiation (red spectrum).

In contrast, the spectrum of the Ni⁰ complex [Ni(dtbbpy)(COD)],^{3c,16} whose deep blue/violet colour ($\lambda_{\text{max}} = 562$ nm in THF) is ascribed to a Ni⁰ to dtbbpy charge-transfer, reveals intense high frequency bands at 1600 cm⁻¹, 1510 cm⁻¹ and 1490 cm⁻¹, which are significantly shifted compared to those of the reduced species of **1** and [Cu(dtbbpy)₂]PF₆ (Figure 3b). Finally, the resonance Raman spectrum of the dtbbpy and BP radical anions recorded in THF were found to be very different to that of photolyzed **1** (Figures S8-S9). Overall, the UV-vis and Raman studies show that UVA photolysis of **1** in MeOH produces a Ni^I complex, in which the nickel ion is bound to at least one dtbbpy, but not to radical anions of BP or dtbbpy.

Further insights on the photoreduction process and structure of the main Ni^I species generated upon photolysis were gained by NMR and EPR studies. The ¹H NMR spectrum of **1** in CD₃OD shows broad resonances characteristic of a paramagnetic species (Figure S10). Using the Evans method,¹⁷ a room temperature magnetic moment $\mu_{\text{eff}} = 2.9 \mu_{\text{B}}$ was measured in CD₃OD, in agreement with the spin-only value of 2.83 μ_{B} expected for a high-spin $S = 1$ Ni^{II} ion, agreeing with a dimer in which the two Ni^{II} ions are not magnetically coupled or, are weakly magnetically coupled. That **1** in solution in MeOH could partly exist as a monomer cannot be ruled out. This would lead to the same magnetic moment. After photolysis, the spectrum of the dark blue-purple solution exhibits intense and well-resolved NMR peaks between 0 and 9 ppm, while the broad resonances of **1** have almost disappeared (Figure 4; the follow-up of the photolysis is given in Figure S10). This shows that the blue-purple reduced Ni^I species, which accumulates upon irradiation, is mainly diamagnetic at room temperature. Since the Ni^I ion (d⁹, $S = 1/2$) is paramagnetic, it means that in the photogenerated reduced species the Ni^I ions are strongly antiferromagnetically coupled to each other. An antiferromagnetic coupling between a Ni^I ion and a BP or dtbbpy radical anion is ruled out by the resonance Raman study. Key structural information

was gained by analysis of the ^1H NMR spectrum combined with COSY (Correlation spectroscopy), HSQC (Heteronuclear single quantum spectroscopy), EXSY (Exchange spectroscopy) and DOSY (Diffusion-ordered spectroscopy) experiments. The dtbbpy ligands in the Ni^{I} complex lie in a non-symmetrical environment as revealed by the splitting of the *t*-Bu resonances and the six resonances observed for the aromatic protons of the bpy (Figure 4a and COSY-HSQC experiments in Figures S11-S12). The BP is present in solution as two main species. One is the free BPCO_2H acid (Figure 4a; Figure S13 for a comparison with an authentic sample; Figure S15 for COSY assignments), which is expected to be formed upon photoreduction. Accordingly, ~ 1 equiv. is present with respect to the $[\text{Ni}^{\text{I}}\text{dtbbpy}]^+$ cation. The second species, characterized by very different chemical shifts and present in stoichiometric amount with respect to dtbbpy, is the BPCO_2 ligand and counterion of the reduced $[\text{Ni}^{\text{I}}\text{dtbbpy}]^+$ cation (Figure 4a; Figure S16 for COSY assignments). This assignment is supported by DOSY measurements (Figure 4b) showing that the dtbbpy and BPCO_2 , which diffuse at the same rate ($D \sim 3.6 \times 10^{-10} \text{ m}^2 \text{ s}^{-1}$), belong to the same species, a species which is significantly larger than the free BPCO_2H which diffuses at a faster rate ($D \sim 4.5 \times 10^{-10} \text{ m}^2 \text{ s}^{-1}$). Photodegradation products of BP, mostly ascribed to the pinacol coupling of BPCO_2H , are also observed by NMR (Figure 4a, Figure S13) and mass spectrometry (Figure S14). Finally, two-dimensional NMR exchange spectroscopy (EXSY) shows that the dtbbpy ligands in the reduced species are kinetically labile, and that the free BPCO_2H is exchanging with the BPCO_2 ligand/counterion (Figure 4c).

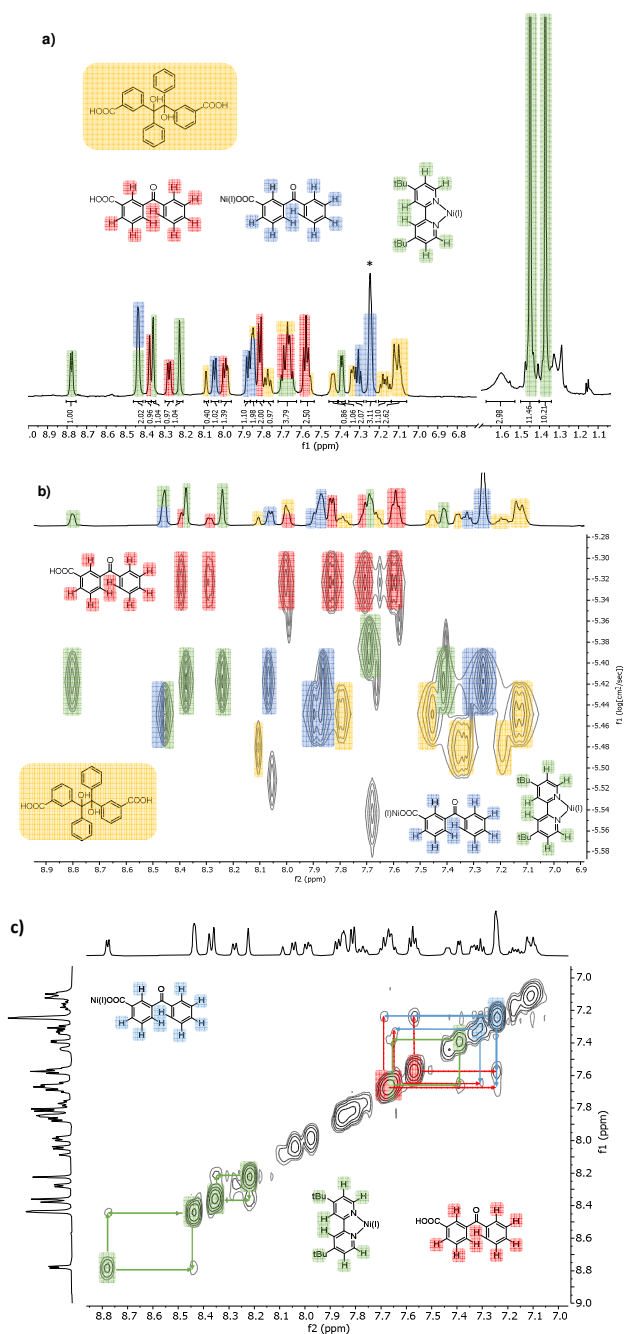


Figure 4. a) ¹H NMR spectrum (600 MHz, recorded at -10 °C) of a CD₃OD solution of **1** (1 mM, 0.7 mL, solution degassed by freeze-pump-thaw cycles followed by flame sealing) irradiated for 120 min with a TLC lamp (320–390 nm) placed at ~ 1 cm of the tube; b) DOSY experiment recorded on the solution of a); c) EXSY experiment (tm = 500 ms) recorded on the solution of a).

X-band EPR spectroscopy has been also used to investigate the mechanism of the photolysis process. Two EPR active Ni^I-based species are rapidly generated during photolysis of **1** but in a very small concentration for both of them (Figure 5a; simulations in Figure S17 and table S2). A rhombic $S = \frac{1}{2}$ EPR spectrum ($g_x = 2.2509$, $g_y = 2.0780$, $g_z = 2.0450$) appears after 1 min of irradiation and almost fully disappeared after 30 min of irradiation. As previously discussed, this transitory signal is tentatively assigned to a mixed-valent $[\text{Ni}^{\text{I/II}}(\text{dtbbpy})_2(\text{BPCO}_2)_3]$ complex as it displays comparable g -values than those reported for the mixed-valent Ni^INi^{II} $[\text{Ni}(\text{pdmt})_2]^-$ complex, and because of the transient electronic absorption band at 890 nm (Figure 2) that is observed in the same region than $[\text{Ni}(\text{pdmt})_2]^-$ (900 nm) and which is characteristic of an intervalence band.¹⁴

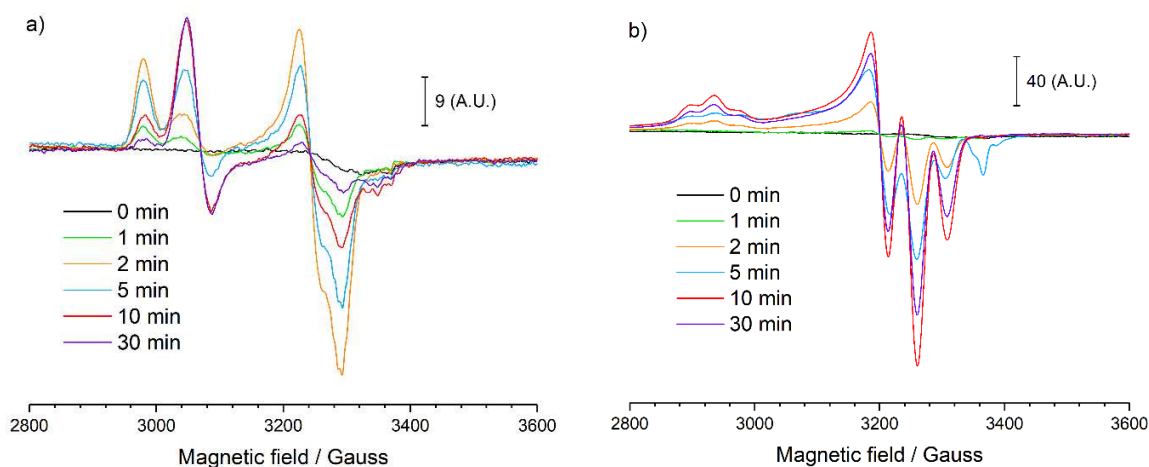
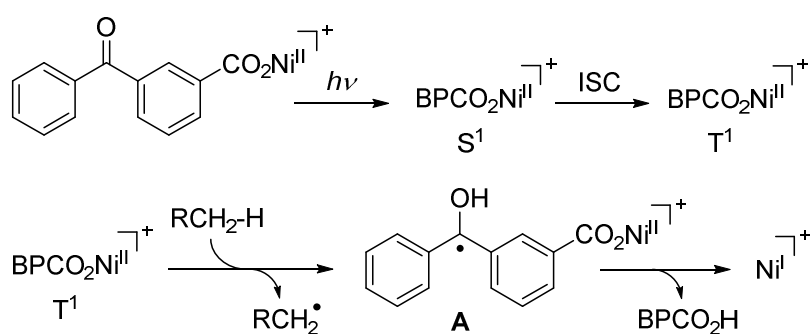


Figure 5. a) EPR spectra (X band, 100 K) of deaerated 0.5 mM MeOH solutions of complex **1** (Six EPR tubes, i.e. one for each irradiation time, were prepared in a glovebox) without irradiation and after 1 min, 2 min, 5 min, 10 min and 30 min of irradiation at 320-390 nm (TLC lamp placed at ~ 1 cm of the tube, irradiation in the glovebox); b) 4 equiv of PBU₃ were added to each EPR tubes after the photolysis (addition in the glovebox) before recording the spectra.

The second observable Ni^I species, characterized by an axial S = 1/2 spectrum ($g_{\text{perp}} = 2.2040$, $g_{\text{para}} = 2.0240$) reaches its maximum concentration between 10 to 30 min of irradiation. It is proposed to correspond to a small amount of the [Ni^I(dtbbpy)₂]⁺ by-product generated during the process. Considering the ¹H NMR study, most of the Ni^I present in the photolyzed solution is expected to be EPR silent. PBU₃ was thus used as a Ni^I trapping agent to evaluate the ratio between silent and EPR active Ni^I species (Figure 5b).¹⁸ Thus, MeOH solutions of **1** have been photolyzed for different times, times after which 4 equiv. of PBU₃ was added. The corresponding solutions display a new EPR spectrum, whose intensity varies as a function of the irradiation time. Hyperfine coupling features arising from the interaction between the unpaired electron and the nucleus of two distinct P atoms (I = 1/2) are observed in this S = 1/2 axial spectrum in both parallel and perpendicular components (Figure 5b). Such a spectrum is characteristic of a mononuclear [LNi^I(PBU₃)₂]⁺ complex (see simulation in Figure S18).¹⁹ As a control experiment, the addition of PBU₃ at t = 0 led to a silent EPR spectrum, showing that the observed [LNi^I(PBU₃)₂]⁺ species is generated from the reaction between the Ni^I species present in the photolyzed solutions and PBU₃, and not from a reduction process driven by PBU₃. Importantly, integration of the signals at 30 min of irradiation before and after addition of PBU₃ revealed that the Ni^I signal is ~ 8 times higher after addition. Interestingly, the comparison of the ¹H NMR spectra of a reduced solution of **1** in CD₃OD before and after addition of PBU₃ (Figures S19, S20) reveals the complete disappearance of the diamagnetic resonances which have been ascribed to the dtbbpy and BPCO₂ ligand resonances of the main Ni reduced species. This result validates the NMR peak attribution of the reduced species (Figure 5), and is also consistent with the breaking of a diamagnetic Ni(I) dimeric complex by PBU₃ to form paramagnetic [dtbbpyNi^I(PBU₃)₂]⁺ species. Thus, most of the Ni^I accumulating upon

photolysis is EPR silent, in agreement with the ^1H NMR and resonance Raman studies, which supports the formation of a diamagnetic species.

Overall, the spectroscopic data strongly suggest that the main reduced species forming during UVA photolysis of **1** in MeOH and *i*-PrOH is a diamagnetic Ni^{I} dimer with general formula $[\text{Ni}_2(\text{dtbbpy})_2(\text{BPCO}_2)_2]$ in which the Ni^{I} ions, most likely bridged by the 3-benzoylbenzoates, are strongly antiferromagnetic coupled through a short Ni-Ni bond, as typically observed in Ni^{I} dimers ($d_{\text{Ni-Ni}} \sim 2.4\text{-}2.5 \text{ \AA}$).²⁰ The Ni^{II} to Ni^{I} reduction process most probably occurs by a PCET (proton coupled electron transfer) from the reducing BP ketyl radical intermediate such as **A** (Scheme 2) that leads to the release of BPCO_2H . The ability of ketyl radicals to reduce transition metals through PCET have been widely exploited to prepare metallic nanoparticles (Au, Cu, Ag...),²¹ or to reduce $\text{Ni}^{\text{II}}(\text{acac})_2$ into $\text{Ni}^{\text{I}}(\text{acac})$.^{18,22} Also, the $\sim -2.2 \text{ V}$ reduction potential measured for the benzophenone radical anion in **1** makes it competent to reduce the Ni^{II} whose reduction potential in **1** occurs at $\sim -1.6 \text{ V}$. The ketyl radical would be generated by classical H-atom abstraction of the solvent from the BP triplet state.



Scheme 2. Proposed Ni^{II} to Ni^{I} photoreduction pathway.

Photolysis in THF. The photoreduction behavior of **1** in THF, which is also a good H-atom donating compound, is markedly different to that observed in alcohols. One should note that when photolysis is conducted in a very poor H-donating solvent such as DCM, no signs of reduction is observed spectroscopically. In THF, a new species is rapidly formed upon photolysis, which exhibits an intense and broad absorption band centered at 505 nm (Figure 6). The species responsible for this absorption is extremely sensitive to O₂, recovery of a colorless solution occurring within seconds when bubbling air. Contrasting with photolysis in alcohols, the only diamagnetic resonances that emerged on the ¹H NMR spectrum during photolysis in THF are those of the 3- benzoylbenzoic acid, as expected if Ni^{II} reduction occurs (Figure S21). The absence of observable resonances from the dtbbpy ligand reveals that it interacts with a reduced paramagnetic Ni species.

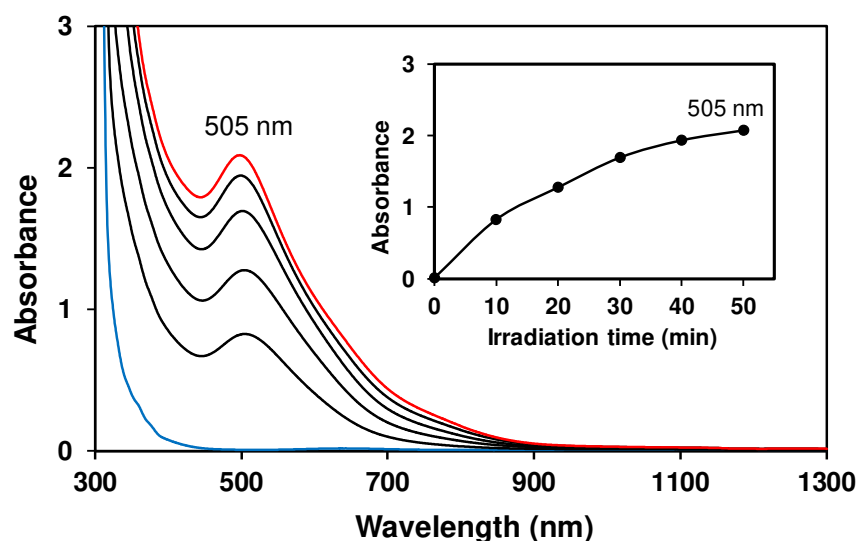


Figure 6. UV-Vis spectra of a THF solution of **1** (0.5 mM, quartz cuvette, path length 1 cm, solution degassed by argon bubbling) after 0 (blue spectrum), 10 min, 20 min, 30 min, 40 min and

50 min (red spectrum) of irradiation (TLC lamp placed at 1 cm of the cuvette). Insert: Evolution of the band maximum with time.

In marked contrast with photoreductions conducted in MeOH, no mononuclear Ni^I species are observed by EPR during photolysis of **1** in THF (Figure S22). Besides, addition of PBU₃ to photolyzed solutions did not generate [LNi^I(PBU₃)_n]⁺, the corresponding EPR spectra remaining silent (Figure S23). Such observations support the rapid formation of a Ni⁰ species upon photolysis of **1** in THF. The band observed at 505 nm could thus be ascribed either (i) to a charge transfer from Ni⁰ to a dtbbpy ligand, albeit the $\lambda_{\text{max}} = 562$ nm of [Ni(dtbbpy)(COD)] in THF is red-shifted by about 50 nm to that of photolyzed **1**,^{3c} or (ii) to the surface plasmon resonance (SPR) of dispersed metallic nickel nano objects. Since the SPR of Ni-based NPs is expected in the UVA region (~ 350 nm),²³ such Ni plasmon resonance shifted at about 500 nm can only be possible if nano objects with extended metallic Ni surfaces, such as aggregated NPs, nanodisks or nanosheets have been formed. Such well-known optical phenomenon is well-established for Au²⁴ or Pd²⁵ metallic nanoobjects. The synthesis and characterization of ultrathin Ni nanosheets has been reported.^{26,27} Their preparation is typically achieved by solvothermal/electrochemical methods from Ni(acac)₂, Ni(formate)₂, Ni(OH)₂ precursors, or from Ni(1,4-benzenedithiol) and Ni(OH)₂ nanosheets. In none of these studies the optical properties of the ultrathin Ni nanosheets have been described. Interestingly, Hillenbrand and coworkers demonstrated that Ni nanodisks prepared on glass substrates by hole-mask colloidal lithography exhibit plasmonic resonances in the visible range, i.e. at ~ 480 nm for 100 nm diameter nickel disks, up to ~ 630 nm for 200 nm diameter nickel disks.²⁸ The far-field extinction spectrum reported for the 100 nm disks is thus closely related to that recorded for the photolyzed solution of **1** in THF (Figure 6).

Strong evidence that ultrathin Ni⁰ nanosheets are formed upon photolysis of **1** in THF came from Raman resonance, DLS and TEM studies. Compared to photolysis in MeOH, the Raman resonance spectrum (λ_{exc} 532 nm) of a photolyzed colorful THF solution (Figure S24) exhibits very weak bands at 1616 cm⁻¹, 1541 cm⁻¹ and ~ 1485 cm⁻¹, supporting the assumption that the band at 500 nm is not due to a Ni^I or Ni⁰ to dtbbpy charge transfer, but rather to a surface plasmon resonance. DLS analysis of burgundy colored and limpid photolyzed THF solutions revealed the presence of colloidal particles with mean size values of ~ 100 nm and ~ 10 μm as shown in the intensity size distribution (Figure 7). It should be mentioned that the largest population is not present when the particle size distribution is weighted in number, which means that the amount of large particles must be negligible in photolyzed THF solutions. In addition, the relatively low scattering intensity of the THF solutions at 90° detection angle evidences an overall low concentration in particles or a poorly light scattering because of a loose structure. The intensity size distribution of the limpid colorless solution obtained after opening the photolyzed solution to air exhibited a similar pattern, but with a significant broadening of the main peaks and the appearance of a new population around 1 μm . Importantly, the aerated limpid and colorless THF solution that was passed through a 0.1 μm PTFE filter did not scatter light, confirming that nano objects with sizes > 100 nm are formed upon photolysis of **1** in THF. As a control experiment, the DLS spectrum of a photolyzed MeOH solution of **1** has been recorded. Its silent spectrum agrees with the formation of a reduced molecular Ni^I complex.

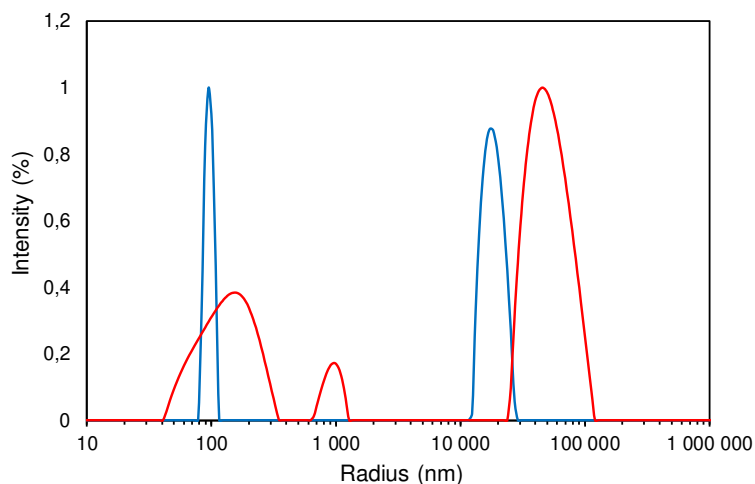


Figure 7. In blue, DLS spectrum of a colorful and limpid THF solution of **1** (0.5 mM, glass test tube, solution degassed by Ar bubbling) recorded after 20 min irradiation (TLC lamp set à 365 nm); In red, DLS spectrum of the limpid and colorless solution obtained after oxygenation of the colored solution with air.

Conclusive evidence that ultrathin nanosheets made of metallic nickel are formed in photolyzed THF solutions have been obtained thanks to transmission electron microscopy (TEM) images, which revealed ultrathin objects of various sizes exhibiting large-area 2D structures (Figure 8). The TEM images, in particular the transparency of some parts of the objects under the electron beam, are highly reminiscent to those previously observed for metallic ultrathin folded nanosheets. However, as previously evidenced by others,^{27c} the nanosheets observed by TEM are most likely Ni(OH)₂ and not Ni⁰ metallic ultrathin sheets due to air oxidation during the transfer of the copper grids to the microscope. Accordingly, the EDS (Energy dispersive spectroscopy) spectrum (Figure 8) and elemental mapping (Figure 9) showed that the nanosheets were mostly composed of nickel and oxygen. With the support of these previous works, our study demonstrates that photolysis of **1** in THF unexpectedly leads to the fast generation of metallic Ni ultrathin nanosheets whose size

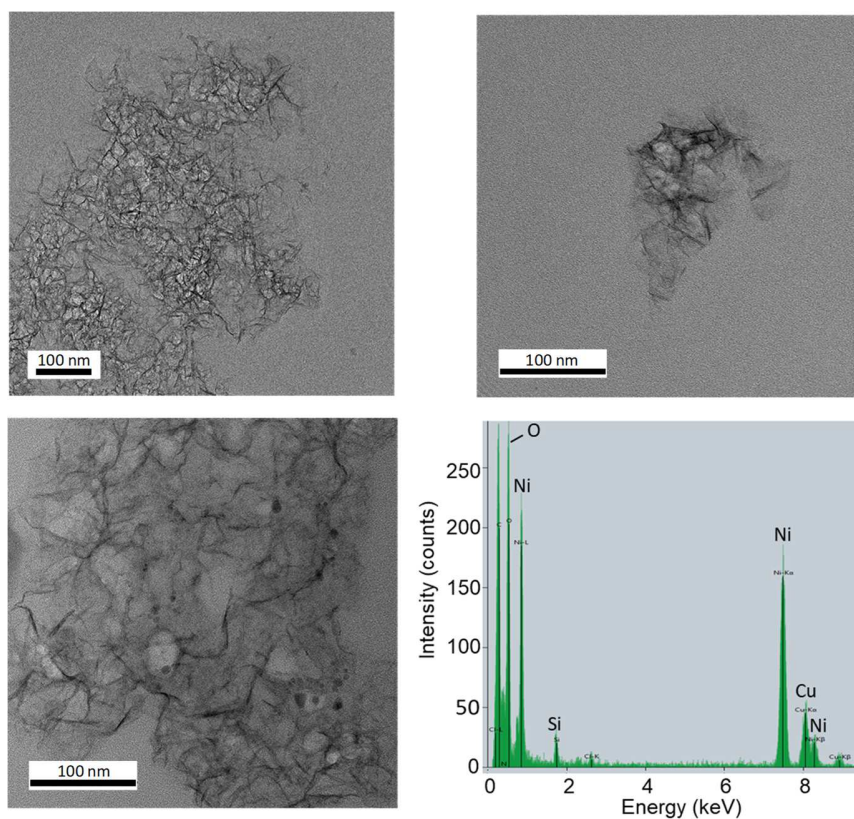


Figure 8. TEM images and EDS spectrum of ultrathin Ni nanosheets. Note that the nanosheets that are observed are most probably Ni(OH)₂ nanosheets resulting from the aerobic oxidation of metallic Ni nanosheets (see text).

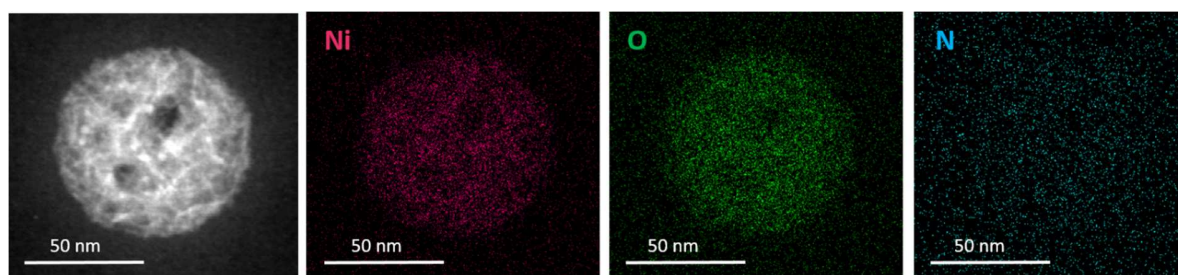


Figure 9. STEM (Scanning Transmission Electron Microscopy) and elemental mapping images of an ultrathin Ni nanosheet (Most probably Ni(OH)₂, see text).

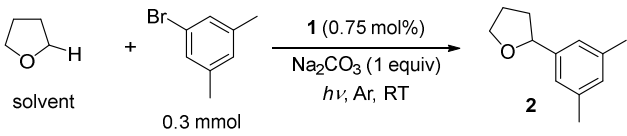
is ~ 100 nm, and which exhibit a SPR at ~ 500 nm, i.e. strongly red-shifted compared to Ni NPs. As for Ni NPs, Ni⁰ nanosheets were shown to display superparamagnetic behavior,^{27a} that could explain why the dtbbpy ligands are not observed on the ¹H NMR spectrum of the photolyzed solution, particularly if bound to the Ni atoms.²⁹ To the best of our knowledge, this is the first example of a photochemical synthesis of metallic nanosheets, and the first report on the SPR properties of Ni ultrathin nanosheets characterized in solution. Even if these O₂-sensitive metallic Ni nanosheets could not be observed directly by TEM, their oxidized forms, most probably as Ni(OH)₂ nanosheets, have been characterized. Further studies that go beyond the objectives of this account will be required to better characterize the magnetic properties of the metallic nanosheets, and elucidate the formation mechanism of such 2D objects, in particular the role of the dtbbpy and/or BPCO₂ ligands on the anisotropic growth. It should be noted that previous studies have reported the formation of Ni(0) nanoparticles by photolysis of NiX₂ salts in the presence of photosensitizers, including carbon nitride,^{30a-c} fluorescein,^{30d} or TiO₂.^{30e} Interestingly, in the course of their study on arylation of esters photocatalyzed by NiCl₂/dtbppy/BIPA/graphitic carbon nitrides, Pieber and coworkers noticed that a small amount of nickel was found as Ni NPs immobilized on the heterogeneous carbon nitrides.^{30b} The same group also showed that the aggregation of Ni(0) NPs into nickel black was responsible for the loss of activity in amine arylations photocatalyzed by a NiX₂/carbon nitrides system.^{30a}

Catalytic studies in relation with proposed mechanisms. With the objective to put into perspective the results of the photolysis study with a key issue raised by previous mechanistic studies of cross-couplings, namely the oxidation state of the catalyst, Ni⁰ vs Ni^I, we tested **1** as precatalyst in two reactions of interest: 1) A C(sp³)-H arylation of THF for which Ni⁰ is proposed

as the catalytic species; 2) An O-arylation of methanol for which Ni^I is proposed as the catalytic species.

C(sp³)-H arylation of THF. In 2018, Martin *et al.* reported the combination of Ni(acac)₂ (10 mol%), a benzophenone with a “push-pull” structure (10 mol%) and the 5,5'-dimethyl-2,2'-bipyridine as ligand (10 mol%) as an optimized precatalytic system to conduct C(sp³)-H arylations and alkylations.^{6c} Arylations/alkylations of the α-C(sp³)-H bonds of cyclic and linear ethers were shown to proceed smoothly under CFL irradiation, typically using ether as solvent. Their mechanistic study supported the mechanism a) of scheme 1, in particular that Ni⁰ is the catalytic species that performs the oxidative addition on the aryl bromides. In support to this, the use of Ni(COD)₂ instead of Ni(acac)₂ led to comparable catalytic activity. Nevertheless, the formation of Ni⁰ species was not demonstrated directly from either the photolyzed Ni^{II} precatalytic system or the LNi^IX catalytic intermediate.

As shown in Table 1, using the conditions developed by Martin (THF as solvent, Na₂CO₃ as the base) the reaction of THF with 1-bromo-3,5-dimethylbenzene in the presence of 0.75 mol% of **1** (1.5 mol% in Ni) affords the coupling product **2** in low to high isolated yields depending on the irradiation source. A low yield of 12% is obtained when using CFL bulbs (entry 1). The yield increases to 42% using low vapor pressure mercury lamps, while using the 365 nm Luzchem LED (Figure S2) a yield up to 76% is obtained (entry 3). For comparison, Martin *et al.* obtained **2** in 96% yield under CFL illumination (60 h) using their precatalytic system Ni(acac)₂ (10 mol%)/ benzophenone (10 mol%) / 5,5'-dimethyl-2,2'-bipyridine (10 mol%).^{6c}

Table 1. C–C cross-coupling photocatalyzed by **1**.

Entry	hv	Time (h)	Yield (%) ^a
1	CFL (23 W) x 2	48	12
2	TLC lamp x2	72	42
3	LED 365 nm Luzchem	72	76

^a Isolated yields. TLC = Thin layer chromatography type lamp (set at 365 nm).
LED = Light emitting diode. CFL = Compact fluorescent light bulb.

Having shown that Ni⁰ is very effectively produced upon photolysis of **1** in THF, and that **1** is catalytically active for the C(sp³)-H arylation of THF under the conditions developed by Martin, these results provide additional support to the mechanistic proposal that involves Ni⁰ as a catalytic species (Scheme 1a). Moreover, considering that Ni^I is inherently an intermediate towards the formation of Ni⁰ from Ni^{II}, our results suggest that the reaction step, which closed the catalytic cycle, i.e. the reduction of LNi^IX into LNi⁰ is likely to occur in THF. Martin proposed that this reduction could be achieved by the benzophenone ketyl radical, thereby regenerating the benzophenone photocatalyst. An alternative process could be the disproportionation of LNi^IX into LNi⁰ and LNi^{II}X₂. In this scenario, the benzophenone would be regenerated by reduction of the LNi^{II}X₂ species produced by the ketyl radical. Previous study by Nocera and coworkers demonstrated that the [Ni^I(bathocuproine)₂]Cl complex, although stable in CH₃CN, disproportionates in THF to afford [Ni⁰(bathocuproine)₂].³¹ Also, a recent work by Doyle and coworkers revealed that a [Ni^I(bpy)Cl] complex disproportionates in THF into [Ni⁰(bpy)₂] and NiCl₂.^{9h} The fact that photolysis of **1** in MeOH led to the stabilization of a [Ni^I(bpy)X₂] species while in THF no Ni^I species were observed but instead Ni⁰ accumulated rapidly could be

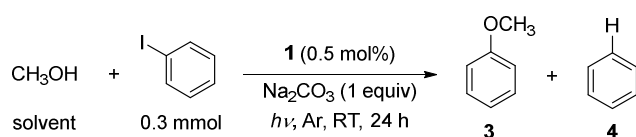
supportive of a disproportionation process that is favored in THF. To test this hypothesis, a deaerated photoreduced MeOH solution of **1** in a UV cuvette was diluted two times with deaerated THF. This led rapidly to the disappearance of the Ni^I dimer absorption bands with the concomitant appearance of a transient species displaying a band at ~ 700 nm (Figure S25). The UV-Vis spectrum recorded 10 min after the addition of THF doesn't show resolved MLCT bands expected for [Ni⁰(dtbbpy)_n] or [Ni^I(dtbbpy)_n]⁺ species. The spectrum is rather characteristic of the presence of nanoparticles diffusing the light over the full visible spectrum. While this experiment shows that the reduced Ni^I dimer is destabilized in the presence of THF and that new species rapidly form, the resulting UV-vis spectra are not informative enough to conclude that this is due to disproportionation. Further studies will be necessary to ascertain this point.

O-arylation of MeOH. In the original work describing O-arylations of alcohols by light-promoted dual Ni/Ir catalysis, a Ni⁰/Ni^{II}/Ni^{III}/Ni^I catalytic cycle was proposed.^{4a} The excited state of the Ir^{III} photocatalyst was intended to oxidize the dtbbpyNi^{II}(alcoxy)(aryl) intermediate to the Ni^{III} oxidation state from which the reductive elimination is favored, with the catalytic cycle closed by the reduction of the Ni^I species by Ir^{II} to generate dtbbpyNi⁰. Recent mechanistic studies have revealed that C-O cross-couplings involving alcohols are most likely photolabile processes proceeding through a “dark” self-sustained Ni^I/Ni^{III} catalytic cycle, with the Ir catalyst there to photoreduce the Ni^{II} precatalyst into catalytically active Ni^I, but also to reduce the Ni^{II} species that may be formed during catalysis, e.g. by comproportionation of Ni^I and Ni^{III}.^{9b,9d}

UVA irradiation of iodobenzene, Na₂CO₃ and 0.5 mol% of **1** in MeOH led to anisole in 80% yield along with 20% of benzene (entry 1). When the reaction is conducted without catalyst or using 2 mol% of 3-benzoylbenzoic acid instead of **1**, no anisole is formed but benzene is obtained in 40% and 26% yields, respectively (entries 2, 3), showing that direct photolysis of iodobenzene competes

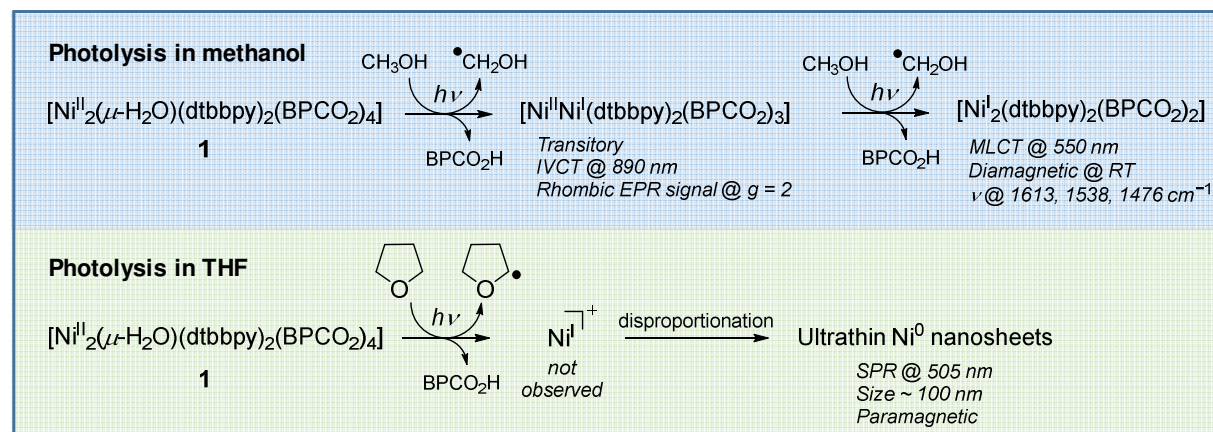
with the Ni-catalyzed cross-coupling. These results, combined with the fact that photolysis of **1** in MeOH produces Ni^I, not Ni⁰, give credence to a mechanism involving a self-sustained photolabile Ni^I/Ni^{III} catalytic cycle such as that occurring in the photopromoted arylation of alcohols by a bpy/Ni^{II}X₂/Ir precatalytic system.^{9b,9d}

Table 2. C–O cross-coupling photocatalyzed by **1**.^a



Entry	Conv. (%) ^b	Yield of 3 (%) ^b	Yield of 4 (%) ^b
1	100	80	20
2 ^c	44	0	40
3 ^d	27	0	26

^a Irradiations conducted with a low-pressure mercury lamp type TLC (thin layer chromatography) set at 365 nm (emission: 320–390 nm). ^b Determined by GC using decane as internal standard. ^c Reaction without catalyst. ^d Reaction using 3-benzoylbenzoic acid (2 mol%) instead of **1**.



Scheme 3. Main results of the photoreduction study of **1**.

CONCLUSION

In summary, the study of the photolysis of **1**, a model complex of the widely used bpy/Ni^{II}X₂/aromatic ketone precatalytic systems in dual photoredox Ni catalysis, provided key insights on the structure and oxidation state of the photogenerated reduced species (Scheme 3). In particular, this study revealed a markedly different behavior whether the photolysis is conducted in MeOH or THF that are both excellent H-atom donors for the BP triplet state, as well as benchmark substrates in C-O or C-C cross-couplings. In MeOH, the accumulated reduced species is a diamagnetic Ni^I dimer of general formula [Ni₂^I(dtbbpy)₂(BPCO₂)₂]. This species is characterized by a Ni^I to dtbbpy charge transfer at 550 nm and a resonance Raman spectrum exhibiting three intense bands at 1613 cm⁻¹, 1538 cm⁻¹ and 1476 cm⁻¹. The NMR study revealed that, 1) the reduced dimer is unsymmetrical in solution, 2) the dtbbpy ligands are kinetically labile while the BPCO₂⁻ ligands can exchange with BPCO₂H released upon Ni^{II} reduction, and 3) BPCO₂H partially degrades during photolysis to form the pinacol product.

The photolysis in THF leads to the fast formation of Ni⁰ which, unexpectedly, accumulates in the form of metallic ultrathin Ni nanosheets with a mean-size of ~ 100 nm. To the best of our knowledge, this is the first direct evidence that Ni⁰ can be generated upon photoirradiation of a bpy/Ni^{II}X₂/aromatic ketone precatalytic system. The metallic ultrathin Ni nanosheets, fully soluble in THF, are characterized by a surface plasmon resonance at 505 nm. When reacting with O₂, the metallic nanosheets are rapidly transformed into colorless oxidized Ni^{II} nanosheets. Contrasting with the photolysis in MeOH, no Ni^I intermediates could be observed or trapped during the reduction process to Ni⁰.

Finally, preliminary catalytic studies showed that **1** is an effective catalyst for light-promoted C-O and C-C cross-couplings between aryl halides and MeOH or THF, respectively. Combined with the photolysis study, our results lend additional weight to the mechanistic hypothesis that the C(sp³)-H bond arylations photo-mediated by a bpy/ Ni^{II}X₂/aromatic carbonyl precatalytic system are catalyzed by a Ni⁰ species. Besides, this study suggests that the O-arylation of alcohols is catalyzed by Ni^I, in agreement with previous studies that have shown that with bpy/Ni^{II}X₂/Ir precatalytic systems such C-O cross-couplings proceed through a self-sustained Ni^I/Ni^{III} catalytic cycle. This contrasts with the Ni⁰/Ni^{II}/Ni^{II*} catalytic cycle suggested for C-nucleophile couplings with bpy/Ni^{II}X₂/aromatic ketones precatalytic systems (scheme 1b). For these reactions, the study of the photoreduction of the precatalyst to determine whether Ni⁰ and/or Ni^I is formed would certainly help to ascertain the proposed mechanisms.

ASSOCIATED CONTENT

Supporting Information.

The following files are available free of charge.

Instruments and methods, synthesis and catalytic experiments, spectra (NMR, UV-Vis, EPR, resonance Raman (PDF)

AUTHOR INFORMATION

Corresponding Author

* Jean-Marc Vincent - Institut des Sciences Moléculaires (ISM), CNRS UMR 5255, Univ. Bordeaux, 33405 Talence, France. Email: jean-marc.vincent@u-bordeaux.fr

Notes

The authors declare no competing financial interest.

ACKNOWLEDGMENT

The Agence Nationale de la Recherche (LightNing project no. ANR-18-CE07-0037-01), the University of Bordeaux and the CNRS are gratefully acknowledged for their financial support. We thank Sabrina Lacomme from the Bordeaux Imaging center for her TEM work on this project. Zidane Mdarhri from the CESAMO analysis platform and Isabelle Pianet from the IRAMAT-CRP2A laboratory are warmly acknowledged for their assistance in the NMR study. Baptiste Abadie is acknowledged for his assistance for the experiment whose results are presented in the Figure S22. This work has benefited from the facilities and expertise of the Biophysical and Structural Chemistry platform (BPCS) at IECB, CNRS UAR 3033, Inserm US001, Bordeaux University.

REFERENCES

(1) Reviews: (a) Zhu, C.; Yue, H.; Chu, L.; Rueping, M. Recent Advances in Photoredox and Nickel Dual-Catalyzed Cascade Reactions: Pushing the Boundaries of Complexity. *Chemical Science* **2020**, *11*, 4051-4064. (b) Milligan, J. A.; Phelan, J. P.; Badir, S. O.; Molander, G. A. Alkyl Carbon-Carbon Bond Formation by Nickel/Photoredox Cross-Coupling. *Angew. Chem. Int. Ed.* **2019**, *58*, 6152-6163. (c) Wenger, O. S. Photoactive Nickel Complexes in Cross-Coupling Catalysis. *Chem. Eur. J.* **2021**, *27*, 2270-2278. d) Yuan, M.; Gutierrez, O. Mechanism, Challenges, and Opportunities of Dual Ni/Photoredox-Catalyzed C(sp²)-C(sp³) Cross-Couplings. *Wires Comp. Mol. Sci.* **2021**, e1573.

(2) Review focusing on stereoselective couplings including dual-catalytic Ni/photoredox processes: Lipp, A.; Badir, S. O.; Molander, G. A. Stereoinduction in Metallophotoredox Catalysis. *Angew. Chem. Int. Ed.* **2021**, *60*, 1714-1726.

(3) Selected examples of C-C cross couplings employing Ir photocatalysts: (a) Tellis, J. C.; Primer, D. N.; Molander, G. A. Single-Electron Transmetalation in Organoboron Cross-Coupling by Photoredo/Nickel Dual Catalysis. *Science* **2014**, *345*, 433-436. (b) Zuo, Z.; Ahneman, D. T.; Chu, L.; Terrett, J. A.; Doyle, A. G.; MacMillan, D. W. C. Merging Photoredox with Nickel Catalysis: Coupling of α -Carboxyl sp^3 -Carbons with Aryl Halides. *Science* **2014**, *345*, 437-440. (c) Shields, B. J.; Doyle, A. G. Direct C(sp^3)-H Cross Coupling Enabled by Catalytic Generation of Chlorine Radicals. *J. Am. Chem. Soc.* **2016**, *138*, 12719-12722. d) El Khatib, M.; Serafim, R. A. M.; Molander, G. A. α -Arylation/Heteroarylation of Chiral α -Aminomethyltrifluoroborates by Synergistic Iridium Photoredox/Nickel Cross-Coupling Catalysis. *Angew. Chem. Int. Ed.* **2016**, *55*, 254-258. e) Heitz, D. R.; Tellis, J. C.; Molander G. A. Photochemical Nickel-Catalyzed C-H Arylation: Synthetic Scope and Mechanistic Investigations. *J. Am. Chem. Soc.* **2016**, *138*, 12715-12718. (f) Johnston, C. P.; Smith, R. T.; Allmendinger, S.; MacMillan, D. W. C. Metallaphotoredox-Catalysed sp^3 - sp^3 Cross-Coupling of Carboxylic Acids with Alkyl Halides. *Nature* **2016**, *536*, 322-325. (g) Corce, V.; Chamoreau, L.-M.; Derat, E.; Goddard, J.-P.; Ollivier, C.; Fensterbank, L. Silicates as Latent Alkyl Radical Precursors: Visible-Light Photocatalytic Oxidation of Hypervalent Bis-Catecholato Silicon Compounds. *Angew. Chem. Int. Ed.* **2015**, *54*, 11414-11418. (h) Nakajima, K.; Nojima, S.; Nishibayashi, Y. Nickel- and Photoredox-Catalyzed Cross-Coupling Reactions of Aryl Halides with 4-Alkyl-1,4-dihydropyridines as Formal Nucleophilic Alkylation Reagents. *Angew. Chem. Int. Ed.* **2016**, *55*, 14106-14110. (i) Zhu, C.; Yue, H. F.; Maity, B.; Atodiresei, I.; Cavallo, L.; Rueping, M. A Multicomponent Synthesis of

Stereodefined Olefins via Nickel Catalysis and Single Electron/Triplet Energy Transfer. *Nat. Catal.* **2019**, *2*, 678-687.

(4) Selected examples of C-heteroatom cross couplings employing Ir photocatalysts: (a) Terrett, J. A.; Cuthbertson, J. D.; Shurtleff, V. W.; MacMillan, D. W. C. Switching on Elusive Organometallic Mechanisms with Photoredox Catalysis. *Nature* **2015**, *524*, 330-334. (b) Corcoran, E. B.; Pirnot, M. T.; Lin, S.; Dreher, S. D.; DiRocco, D. A.; Davies, I. W.; Buchwald, S. L.; MacMillan D. W. C. Aryl Amination Using Ligand-Free Ni(II) Salts and Photoredox Catalysis. *Science* **2016**, *353*, 279-283. (c) Oderinde, M. S.; Jones, N. H.; Juneau, A.; Frenette, M.; Aquila, B.; Tentarelli, S.; Robbins, D. W.; Johannes, J. W. Highly Chemoselective Iridium Photoredox and Nickel Catalysis for the Cross-Coupling of Primary Amines with Aryl Halides. *Angew. Chem.* **2016**, *128*, 13413-13417. (d) Oderinde, M. S.; Frenette, M.; Robins, D. W.; Aquila, B.; Johannes, J. W. Photoredox Mediated Nickel Catalyzed Cross-Coupling of Thiols With Aryl and Heteroaryl Iodides via Thyl Radicals. *J. Am. Chem. Soc.* **2016**, *138*, 1760-1763. (e) Welin, E. R.; Le, C.; Arias-Rotondo, D. M.; McCusker, J. K.; MacMillan, D. W. C. Photosensitized, Energy Transfer-Mediated Organometallic Catalysis Through Electronically Excited Nickel(II). *Science* **2017**, *355*, 380-385. (f) Kim, T.; McCarver, S. J.; Lee, C.; MacMillan, D. W. C. Sulfonamidation of Aryl and Heteroaryl Halides through Photosensitized Nickel Catalysis. *Angew. Chem. Int. Ed.* **2018**, *57*, 3488-3492. (g) Zhu, Y. Y.; Lan, G.; Fan, Y.; Veroneau, S. S.; Song, Y.; Micheroni, D.; Lin, W. Merging Photoredox and Organometallic Catalysts in a Metal-Organic Framework Significantly Boosts Photocatalytic Activities. *Angew. Chem. Int. Ed.* **2018**, *57*, 14090-14094. (h) Lan, G.; Quan, Y.; Wang, M.; Nash, G. T.; You, E.; Song, Y.; Veroneau, S. S.; Jiang, X.; Lin, W. Metal-Organic Layers as Multifunctional Two-Dimensional Nanomaterials for Enhanced Photoredox Catalysis. *J. Am. Chem. Soc.* **2019**, *141*, 15767-15772.

(5) Review focusing on carbonyl-photoredox/metal dual catalysis: Zhu, D.-L.; Young, D. J.; Li, H.-X. Carbonyl-Photoredox/Metal Dual Catalysis: Applications in Organic Synthesis. *Synthesis* **2020**, *52*, 3493-3510.

(6) Selected examples of C-C cross couplings employing organic photocatalysts: (a) Meng, Q.-Y.; Wang, S.; König, B. Carboxylation of Aromatic and Aliphatic Bromides and Triflates with CO₂ by Dual Visible-Light-Nickel Catalysis. *Angew. Chem. Int. Ed.* **2017**, *56*, 13426-13430. (b) Masuda, Y.; Ishida, N.; Murakami, M. Aryl Ketones as Single-Electron-Transfer Photoredox Catalysts in the Nickel-Catalyzed Homocoupling of Aryl Halides. *Eur. J. Org. Chem.* **2016**, 5822-5825. (c) Shen, Y.; Gu, Y.; Martin, R. *sp*³ C-H Arylation and Alkylation Enabled by the Synergy of Triplet Excited ketones and Nickel Catalysts. *J. Am. Chem. Soc.* **2018**, *140*, 12200-12209. (d) Dewanji, A.; Krach, P. E.; Rueping, M. The dual Role of Benzophenone in Visible-Light/Nickel Photoredox-Catalyzed C-H Arylations: Hydrogen-Atom Transfer and Energy Transfer. *Angew. Chem. Int. Ed.* **2019**, *58*, 3566-3570. (e) Zhang, L.; Si, X.; Yang, Y.; Zimmer, M.; Witzel, S.; Sekine, K.; Rudolph, M.; Hashmi, A. S. K. The Combination of Benzaldehyde and Nickel-Catalyzed Photoredox C(*sp*³)-H Alkylation/Arylation. *Angew. Chem. Int. Ed.* **2019**, *58*, 1823-1827. (f) Schirmer, T. E.; Wimmer, A.; Weinzierl, F. W. C.; König, B. Photo-Nickel Dual Catalytic Benzoylation of Aryl Bromides. *Chem. Commun.* **2019**, *55*, 10796-10799. (g) Ishida, N.; Masuda, Y.; Imamura, Y.; Yamazaki, K.; Murakami, M. Carboxylation of Benzylic and Aliphatic C-H Bonds with CO₂ Induced by Light/Ketone/Nickel. *J. Am. Chem. Soc.* **2019**, *141*, 19611-19615. (h) Campbell, M. W.; Yuan, M.; Polites, V. C.; Gutierrez, O.; Molander, G. Photochemical C-H Activation Enables Nickel-Catalyzed Olefin Dicarbofunctionalization. *J. Am. Chem. Soc.* **2021**, *143*, 3901-3910. (i) Zhu, D.-L. Zhu; Xu, R.; Wu, Q.; Li, H.-Y.; Lang, J.; Li, H.-X. Nickel-

Catalyzed Sonogashira C(sp)-C(sp²) Coupling through Visible-Light Sensitization. *J. Org. Chem.* **2020**, *85*, 9201-9212.

(7) Selected examples of C-heteroatom cross couplings employing organic photocatalysts: (a) Ding, W.; Lu, L.-Q.; Zhou, Q.-Q.; Wei, Y.; Chen, J.-R.; Xiao, W.-J. Bifunctional Photocatalysts for Enantioselective Aerobic Oxidation of β -Ketoesters. *J. Am. Chem. Soc.* **2017**, *139*, 63-66. (b) Du, Y.; Pearson, R. M.; Lim, C.-H.; Sartor, S. M.; Ryan, M. D.; Yang, H.; Damrauer, N. H.; Miyake, G. M. Strongly Reducing, Visible-Light Organic Photoredox Catalysts as Sustainable Alternative to Precious Metals. *Chem. Eur. J.* **2017**, *23*, 10962-10968. (c) Yang, L.; Huang, Z.; Li, G.; Zhang, W.; Cao, R.; Wang, C.; Xiao, J.; Xue, D. Synthesis of Phenol: Organophotoredox/Nickel Dual Catalytic Hydroxylation of Aryl Halides with Water. *Angew. Chem. Int. Ed.* **2018**, *57*, 1968-1972. (d) Lu, J.; Pattengale, B.; Liu, Q.; Yang, S.; Shi, W.; Li, S.; Huang, J.; Zhang, J. Donor-Acceptor Fluorophores for Energy-Transfer-Mediated Photocatalysis. *J. Am. Chem. Soc.* **2018**, *140*, 13719-13725. (e) Jiang, S.; Zhang, Z.-T. Young, D. J.; Chai, L.-L.; Wu, Q.; Li, H.-X. Visible-Light Mediated Cross-Coupling of Aryl Halides with Sodium Sulfinates via Carbonyl-Photoredox/Nickel Dual Catalysis. *Org. Chem. Front.* **2022**, doi.org/10.1039/D1QO01850G. (f) Zhu, D.-L.; Jiang, S.; Wu, Q.; Wang, H.; Li H.-Y.; Li, H.-X. Nickel-Catalyzed Etherification of Phenols and Aryl Halides through Visible-Light-Induces Energy Transfer. *Org. Lett.* **2021**, *23*, 8327-8332. (g) Zhu, D.-L.; Jiang, S.; Wu, Q.; Wang, H.; Chai, L.-L.; Li, H.-Y.; Li, H.-X. Visible-Light-Induced Nickel-Catalyzed P(O)-C(sp²) Coupling Using Thioxanthen-9-one as a Photoredox Catalysis. *Org. Lett.* **2021**, *23*, 160-165. (h) Zhu, D.-L.; Li, H.-X.; Xu, Z.-M.; Li, H.-Y.; Young, D. J.; Lang, J.-P. Visible Light Driven, Nickel-Catalyzed Aryl Esterification using a Triplet Photosensitizer Thioxanthen-9-one. *Org. Chem. Front.* **2019**, *6*, 2353-2359.

(8) Energy transfer to/photoexcitation of Ni-amine complexes: (a) Shields, B. J.; Kudisch, B.; Scholes, G. D.; Doyle, A. G. Long-Lived Charge-Transfer States of Nickel(II) Aryl Halide Complexes Facilitate Bimolecular Photoinduced Electron Transfer. *J. Am. Chem. Soc.* **2018**, *140*, 3035-3039. (b) Kudisch, M.; Lim, C.-H.; Thordarson, P.; Miyake, G. M. Energy Transfer to Ni-Amine Complexes in Dual Catalytic, Light-Driven C-N Cross-Coupling Reactions. *J. Am. Chem. Soc.* **2019**, *141*, 19479-19486. (c) Lim, C.-H.; Kudisch, M.; Liu, B.; Miyake, G. M. C-N Cross-Coupling via Photoexcitation of Nickel-Amine Complexes. *J. Am. Chem. Soc.* **2018**, *140*, 7667-7673. (d) Tian, L.; Till, N. A.; Kudisch, B.; MacMillan, D. W. C.; Scholes, G. D. Transient Absorption Spectroscopy Offers Mechanistic Insights for a Iridium/Nickel-Catalyzed C-O Coupling. *J. Am. Chem. Soc.* **2020**, *142*, 4555-4559. (e) Ting, S. I.; Garakyaraghi, S.; Taliaferro, C. M.; Shields, B. J.; Scholes, G. D.; Castellano, F. N.; Doyle, A. G. ^3d-d Excited States of Ni(II) Complexes Relevant to Photoredox Catalysis: Spectroscopic Identification and Mechanistic Implications. *J. Am. Chem. Soc.* **2020**, *142*, 5800-5810; (f) Cagan, D. A.; Bím, D.; Silva, B.; Kazmierczak, N. P.; McNicholas, B. J.; Hadt, R. G. Elucidating the Mechanism of Excited-State Bond Homolysis in Nickel-Bipyridine Photoredox Catalysts. *J. Am. Chem. Soc.* **2022**, *144*, 6516-6531.

(9) Ni^I/Ni^{III} cycle for the oxidative addition/reductive elimination steps: (a) Kalvet, I.; Guo, Q.; Tizzard, G. J.; Schoenebeck, F. When Weaker Can Be Tougher: The Role of Oxidation State (I) in P- vs N-Ligand-Derived Ni-Catalyzed Trifluoromethylthiolation of Aryl Halides. *ACS Catal.* **2017**, *7*, 2126-2132. (b) Sun, R.; Qin, Y.; Ruccolo, S.; Schnedermann, C.; Costentin, C.; Nocera, D. G. Elucidation of a Redox-Mediated Reaction Cycle for Nickel-Catalyzed Cross Coupling. *J. Am. Chem. Soc.* **2019**, *141*, 89-93. (c) Till, N. A.; Tian, L.; Dong, Z.; Scholes, G. D.; MacMillan, D. W. C. Mechanistic Analysis of Metallaphotoredox C-N Coupling: Photocatalysis Initiates and

Perpetuates Ni(I)/Ni(III) Coupling Activity. *J. Am. Chem. Soc.* **2020**, *142*, 15830-15841. (d) Sun, R.; Qin, Y.; Nocera, D. G. General Paradigm on Photoredox Nickel-Catalyzed Cross-Coupling Allows for Light-Free Access to Reactivity. *Angew. Chem. Int. Ed.* **2020**, *59*, 9527-9533. (e) Till, N. A.; Oh, S.; MacMillan, D. W. C.; Bird, M. J. The Application of Pulse Radiolysis to the Study of Ni(I) Intermediates in Ni-Catalyzed Cross-Coupling Reactions. *J. Am. Chem. Soc.* **2021**, *143*, 9332-9337. (f) Qin, Y.; Sun, R.; Gianoulis, N. P.; Nocera, D. G. Photoredox Nickel-Catalyzed C-S Cross-Coupling: Mechanism, Kinetics and Generalization *J. Am. Chem. Soc.* **2021**, *143*, 2005-2015. (g) Ren, H.; Li, G.-F.; Zhu, B.; Lv, X.-D.; Yao, L.-S.; Wang, X.-L.; Su, Z.-M.; Guan, W. How Does Iridium(III) Photocatalyst Regulate Nickel(II) Catalysts on Metallaphotoredox-Catalyzed C-S Cross-Coupling? Theoretical and Experimental Insights. *ACS Catal.* **2019**, *9*, 3858-3865. (h) Ting, S. L.; Williams, W. L.; Doyle, A. G. Oxidative Addition of Aryl Halides to a Ni(I)-Bipyridine Complex. *J. Am. Chem. Soc.* **2022**, *144*, 5575-5582. (i) Na, H.; Mirica, L. M. Deciphering the Mechanism of the Ni-Photocatalyzed C-O Cross-Coupling Reaction Using a Tridentate Pyridinophane Ligand. *Nat. Commun.* **2022**, *13*, 1313.

(10) Radical trapping: (a) Yuan, M.; Song, Z.; Badir, S. O.; Molander, G. A.; Gutierrez, O. On the Nature of C(sp³)-C(sp²) Bond Formation in Nickel-Catalyzed Tertiary Radical Cross-Couplings: A Case Study of Ni/Photoredox Catalytic Cross-Coupling of Alkyl Radicals and Aryl Halides. *J. Am. Chem. Soc.* **2020**, *142*, 7225-7234. (b) Maity, B.; Zhu, C.; Yue, H.; Huang, L.; Harb, M.; Minenkov, Y.; Rueping, M.; Cavallo, L. Mechanistic Insight into the Photoredox-Nickel-HAT Triple Catalyzed Arylation and Alkylation of α -Amino C_{sp³}-H Bonds. *J. Am. Chem. Soc.* **2020**, *142*, 16942-16952. (c) Malik, J. A.; Madani, A.; Pieber, B.; Seeberger, P. H. Evidence of Photocatalyst Involvement in Oxidative Additions of Ni-Catalyzed Carboxylate O-Arylations. *J. Am. Chem. Soc.* **2020**, *142*, 11042-11049.

- (11) (a) Harmand, L.; Cadet, S.; Kauffmann, B.; Scarpantonio, L.; Batat, P.; Jonusauskas, G.; McClenaghan, N. D.; Lastécouères, D.; Vincent, J.-M. Copper Catalyst Activation Driven by Photoinduced Electron Transfer: A Prototype Photolabile Click Catalyst. *Angew. Chem. Int. Ed.* **2012**, *51*, 7137-7141. (b) Harmand, L.; Lambert, R.; Scarpantonio, L.; McClenaghan, N. D.; Lastécouères, D.; Vincent, J.-M. A Photoreducible Copper(II)-Tren Complex of Practical Value: Generation of a Highly Reactive Click Catalyst. *Chem. Eur. J.* **2013**, *19*, 16231-16239. (c) Beniazza, R.; Lambert, R.; Harmand, L.; Molton, F.; Duboc, C.; Denisov, S.; Jonusauskas, G.; McClenaghan, N. D.; Lastécouères, D.; Vincent, J.-M. Sunlight-Driven Copper-Catalyst Activation Applied to Photolabile Click Chemistry. *Chem. Eur. J.* **2014**, *20*, 13181-13187.
- (12) Beniazza, R.; Molton, F.; Duboc, C.; Tron, A.; McClenaghan, N. D.; Lastécouères, D.; Vincent, J.-M. Copper(I)-Photocatalyzed Trifluoromethylation of Alkenes. *Chem. Commun.* **2015**, *51*, 9571-9574.
- (13) (a) Abadie, B.; Jardel, D.; Pozzi, G.; Toullec, P.; Vincent, J.-M. Dual Benzophenone/Copper-Photocatalyzed Giese-Type Alkylation of C(sp³)-H Bonds. *Chem. Eur. J.* **2019**, *25*, 16120-16127. (b) Abadie, B.; Jonusauskas, G.; McClenaghan, N. D.; Toullec, P.; Vincent, J.-M. Alkylation of the α -amino C-H Bonds of Anilines Photocatalyzed by a DMEDA-Cu-Benzophenone Complex: Reaction Scope and Mechanistic Studies. *Org. Biomol. Chem.* **2021**, *19*, 5800-5805.
- (14) Krüger, H.-J.; Holm, R. H. Chemical and Electrochemical Reactivity of Nickel(II,I) Thiolate Complexes: Examples of Ligand-Based Oxidation and Metal-Centered Oxidative Addition. *Inorg. Chem.* **1989**, *28*, 1148-1155.
- (15) Bradley, P. G.; Kress, N.; Hornberger, B. A.; Dallinger, R. F.; Woodruff, W. H. Vibrational Spectroscopy of the Electronically Excited State. 5. Time-Resolved Resonance Raman Study of

tris(bipyridine)ruthenium(II) and Related Complexes. Definitive Evidence for the “Localized” MLCT State. *J. Am. Chem. Soc.* **1981**, *103*, 7441-7446.

(16) King, A. E.; Stieber, S. C. E.; Henson, N. J.; Kozimor, S. A.; Scott, B. L.; Smythe, N. C.; Sutton, A. D.; Gordon, J. C. Ni(bpy)(cod): A Convenient Entryway into the Efficient Hydroboration of Ketones, Aldehydes and Imines. *Eur. J. Inorg. Chem.* **2016**, 1635-1640.

(17) Evans, D. F. The Determination of the Paramagnetic Susceptibility of Substances in Solution by Nuclear Magnetic Resonance. *J. Chem. Soc.* **1959**, 2003–2005.

(18) Chow, Y. L.; Buono-Core, G. E.; Lee, C. W. B.; Scaiano, J. C. Sensitized Photoreduction of Bis(acetylacetonato)nickel(II) by Triplet-State Aromatic Ketones. *J. Am. Chem. Soc.* **1986**, *108*, 7620-7627.

(19) Saraev, V. V.; Kraikivskii, P. B.; Matveev, D. A.; Zelinskii, S. N.; Lammertsma, K. EPR Study of the Oxidation Reaction of Nickel(0) Phosphine Complexes with Lewis and Brønsted Acids. *Inorg. Chim. Acta* **2006**, *359*, 2314-2319.

(20) Selected examples: (a) Somerville, R. J.; Hale, L. V. A.; Gómez-Bengoa, E.; Burés, J.; Martin, R. Intermediacy of Ni-Ni Species in sp^2 C-O Bond Cleavage of Aryl Esters: Relevance in Catalytic C-Si Bond Formation. *J. Am. Chem. Soc.* **2018**, *140*, 8771-8780. (b) Beck, R.; Johnson, S. A. Dinuclear Ni(I)-Ni(I) Complexes with Syn-Facial Bridging Ligands from Ni(I) Precursors or Ni(II)/Ni(0) Comproportionation. *Organometallics* **2013**, *32*, 2944-2951. (c) Dible, B. R.; Sigman, M. S.; Arif, A. M. Oxygen-Induced Ligand Dehydrogenation of a Planar Bis- μ -Chloronickel(I) Dimer Featuring an NHC Ligand. *Inorg. Chem.* **2005**, *44*, 3774-3776. (d) Bach, I.; Goddard, R.;

Kopiske, C.; Seevogel, K.; Pörschke, K.-R. Synthesis, Structure and Reactivity of $(^t\text{Bu}_2\text{PC}_2\text{H}_4\text{PtBu}_2)\text{Ni}(\text{CH}_3)_2$ and $\{(^t\text{Bu}_2\text{PC}_2\text{H}_4\text{PtBu}_2)\text{Ni}\}_2(\mu\text{-H})_2$. *Organometallics* **1999**, *18*, 10-20.

(21) Scaiano, J. C.; Stampelcoskie, K. G.; Hallett-Tapley, G. L. Photochemical Norrish Type I Reaction as a Tool for Metal Nanoparticle Synthesis: Importance of Proton Coupled Electron Transfer. *Chem. Commun.* **2012**, *48*, 4798-4808.

(22) Ishida, N.; Kamae, Y.; Murakami, M. Preparation of $\text{Ni}(\text{cod})_2$ Using Light as the Source of Energy. *Organometallics* **2019**, *38*, 1413-1416.

(23) Creighton, J. A.; Eadon, D. G. Ultraviolet-Visible Absorption Spectra of the Colloidal Metallic Elements. *J. Chem. Soc. Faraday Trans.* **1991**, *87*, 3881-3891.

(24) (a) Ghosh, S. K.; Pal, T. Interparticle Coupling Effect on the Surface Plasmon Resonance of Gold Nanoparticles: From Theory to Applications. *Chem. Rev.* **2007**, *107*, 4797-4862. (b) Huang, X.; El-Sayed, M. A. Gold Nanoparticles: Optical Properties and Implementations in Cancer Diagnosis and Photothermal Therapy. *J. Adv. Res.* **2010**, *1*, 13-28.

(25) (a) Huang, X.; Tang, S.; Mu, X.; Dai, Y.; Chen, G.; Zhou, Z.; Ruan, F.; Yang, Z.; Zheng, N. Freestanding Palladium Nanosheets with Plasmonic and Catalytic Properties. *Nat. Nanotechnol.* **2011**, *6*, 28-32. (b) De Marchi, S.; Núñez-Sánchez, S.; Bodelón, G.; Pérez-Juste, J.; Pastoriza-Santos, I. Pd Nanoparticles as a Plasmonic Material: Synthesis, Optical Properties and Applications. *Nanoscale* **2020**, *12*, 23424-23443.

(26) Reviews on ultrathin two-dimensional metallic nanocrystals/nanosheets: (a) Luo, M.; Yang, Y.; Sun, Y.; Qin, Y.; Li, C.; Li, Y.; Li, M.; Zhang, S.; Su, D.; Guo, S. Ultrathin Two-Dimensional Metallic Nanocrystals for Renewable Energy Electrocatalysis. *Mater. Today* **2019**, *23*, 45-56. (b)

Yu, Q.; Yang, Y. Synthesis of Two-Dimensional Metallic Nanosheets: From Elemental Metal to Chemically Complex Alloys. *ChemNanoMat* **2020**, *6*, 1683-1711.

(27) Selected articles focusing on Ni nanosheets: (a) Leng, Y.; Zhang, Y.; Liu, T.; Suzuki, M.; Li, X. Synthesis of Single Crystalline Triangular and Hexagonal Ni Nanosheets with Enhanced Magnetic Properties. *Nanotechnology* **2006**, *17*, 1797-1800. (b) Kuang, Y.; Feng, G.; Li, P.; Bi, Y.; Li, Y.; Sun, X. Single-Crystalline Ultrathin Nickel Nanosheets Array from In Situ Topotactic Reduction for Reactive and Stable Electrocatalysis. *Angew. Chem. Int. Ed.* **2016**, *55*, 693-697. (c) Hu, C.; Ma, Q.; Hung, S.-F.; Chen, Z.-N.; Ou, D.; Ren, B.; Chen, H. M.; Fu, G.; Zheng, N. In Situ Electrochemical Production of Ultrathin Nickel Nanosheets for Hydrogen Evolution. *Chem* **2017**, *3*, 122-133. (d) Ni, W.; Wang, B.; Cheng, J.; Li, X.; Guan, Q.; Gu, G.; Huang, L. Hierarchical Foam of Exposed Ultrathin Nickel Nanosheets Supported on Chainlike Ni-Nanowires and the derivative Chalcogenide for Enhanced Pseudocapacitance. *Nanoscale* **2014**, *6*, 2618-2623. (e) Yu, J.-W.; Wang, X.-Y.; Yuan, C.-Y.; Li, W.-Z.; Wang, Y.-H.; Zhang, Y.-W. Synthesis of Ultrathin Ni Nanosheets for Semihydrogenation of Phenylacetylene to Styrene Under Mild Conditions. *Nanoscale* **2018**, *10*, 6936-6944. (f) Dai, L.; Chen, Z.-N.; Li, L.; Liu, Z.; Zhang, H. Ultrathin Ni(0)-Embedded Ni(OH)₂ Heterostructured Nanosheets with Enhanced Electrochemical Overall Water Splitting. *Adv. Mater.* **2020**, *32*, 1906915.

(28) Chen, J.; Albella, P.; Pirzadeh, Z.; Alonso-González, P.; Huth, F.; Bonetti, S.; Bonanni, V.; Åkerman, J.; Nogués, J.; Vavassori, P.; Dmitriev, A.; Aizpurua, J.; Hillenbrand, R. Plasmonic Nickel Nanoantennas. *Small* **2011**, *7*, 2341-2347.

(29) Selected article describing metallic NPs stabilized by bipyridine ligands: (a) Dykeman, R. R.; Yan, N.; Scopelliti, R.; Dyson, P. J. Enhanced Rate of Arene Hydrogenation with Imidazolium

Functionalized Bipyridine Stabilized Rhodium Nanoparticle Catalysts. *Inorg. Chem.* **2011**, *50*, 717-719. (b) Léger, B.; Denicourt-Nowicki, A.; Olivier-Bourbigou, H.; Roucoux, A. Rhodium Nanocatalysts Stabilized by Various Bipyridine Ligands in Nonaqueous Ionic Liquids: Influence of the Bipyridine Coordination Modes in Arene Catalytic Hydrogenation. *Inorg. Chem.* **2008**, *47*, 9090-9096.

(30) (a) Gisbertz, S.; Reischauer, S.; Pieber, B. Overcoming Limitations in Dual Photoredox/Ni-Catalyzed C-N Cross-Couplings Due to Catalyst Deactivation. *Nat. Catal.* **2020**, *3*, 611-620. (b) Pieber, B.; Malik, J. A.; Cavedon, C.; Gisbertz, S.; Savateev, A.; Cruz, D.; Heil, T.; Zhang, G.; Seeberger, P. H. Semi-heterogeneous Dual Ni/Photocatalysis using Carbon Nitrides: Esterification of Carboxylic Acids with Aryl Halides. *Angew. Chem. Int. Ed.* **2019**, *58*, 9575-9580. (c) Indra, A.; Menezes, P. W.; Kailasam, K.; Hollmann, D.; Schröder, M.; Thomas, A.; Brückner, A.; Driess, M. Nickel as a Co-Catalyst for Photocatalytic Hydrogen Evolution on Graphitic-Carbon Nitride (sg-CN): What is the nature of the active species? *Chem. Commun.* **2016**, *52*, 104-107. (d) Wang, C.; Cao, S.; Fu W.-F. A Stable Dual-Functional System of Visible-Light-Driven Ni(II) Reduction to a Nickel Nanoparticle Catalyst and Robust *in situ* Hydrogen Production. *Chem. Commun.* **2013**, *49*, 11251-11253. (e) Rodríguez, J. L.; Valenzuela, M. A.; Pola, F.; Tiznado, H.; Poznyak, T. Photodeposition of Ni Nanoparticles on TiO₂ and their Application in the Catalytic Ozonation of 2,4-dichlorophenoxyacetic Acid. *J. Mol. Catal. A: Chem.* **2012**, *353-354*, 29-36.

(31) Powers, D. C.; Anderson, B. L.; Nocera, D. G. Two-Electron HCl to H₂ Photocycle Promoted by Ni(II) Polypyridyl Halide Complexes. *J. Am. Chem. Soc.* **2013**, *135*, 18876-18883.